Seismic Attributes Analysis as a Precursor for Hydrocarbon Indication: A Case Study of Onshore Fuba field, Niger Delta, Nigeria

U. Ochoma*

Department of Physics, Rivers State University, P.M.B 5080, Port Harcourt, Nigeria.
*Email: umaocho@gmail.com**

ABSTRACT

Seismic attributes analysis as a precursor for hydrocarbon indication in onshore Fuba Field, Niger Delta, Nigeria using Well-logs and 3D Seismic data are here presented. Well-to-seismic ties, faults and horizon mapping, time-surface generation, depth conversion and seismic attributes generation were carried out using Petrel software. The structural interpretation of seismic data reveal highly synthetic and antithetic faults which are in line with faults trends identified in the Niger Delta. Of the 36 interpreted faults, only synthetic and antithetic faults are regional, running from the top to bottom across the field. These faults play significant roles in trap formation at the upper, middle and lower sections of the field. Three distinct horizons were mapped. Reservoir M is found at a shallower depth from 10937 to 10997 ft, reservoir N is found at a depth ranging from 11213 to 11241 ft while reservoir O is found at a deeper depth ranging from 11681 to 11871 ft respectively. Analysis of the relevant seismic attributes such as variance edge, root mean square, maximum amplitude and relative acoustic impedance were applied to the seismic data. The variance values ranges from 0.0 to 1.0. The Variance edge analysis was used to delineate the prominent and subtle faults in the area. The RMS amplitude values ranges from 9,000 to 13,000 in the reservoirs. The root mean square amplitude and maximum amplitude analysis reveal bright spot anomaly. These amplitude anomalies served as direct hydrocarbon indicators (DHIs), unravelling the presence and possible hydrocarbon prospective zones. The relative acoustic impedance analysis was used for delineating lithology variation in the seismic sections. Results from this study have shown that away from the currently producing zone of the field, additional leads and prospects exist, which could be further evaluated for hydrocarbon production.

Keywords: Seismic attributes, Root mean square amplitude, Maximum amplitude, Niger Delta, Nigeria.

1.0. Introduction

Seismic attributes are quantitative measures of seismic characteristics of interest (Liner, 2004; Oyeyemi, and Aizebeokhai, 2015; Adewoye, et al, 2015). Seismic attributes need to be integrated in some interpretations as they can be used as tools for predicting reservoir geometry and possibly displaying lateral changes in thickness including fluid contacts (Steiner, and Lockhart, 1988). Seismic attributes analysis involves the procedure used to extract corresponding subsurface geological information from seismic sections (Allstair, 2011; Avseth, et al, 2005). Structural and stratigraphic traps could be very subtle and are therefore difficult to map accurately (Omoja, and Obiekezie, 2019). The geometrical attributes are used for structural and stratigraphic interpretations of seismic data. Seismic attributes are widely used for detection of hydrocarbon reservoirs (Pramanik, et al, 2002; Van, 2000; Vig et al, 2002). Improved methodologies are needed to discriminate between true hydrocarbon indicators and non-indicators by imaging the detail subsurface structure with a view to delineate new hydrocarbon zones that might be hidden in structural traps for the development programmes of the field. Seismic attributes analysis being an integral part of 3D seismic interpretation is one of these advancements (Chopra, and Marfurt, 2005). Several researchers have made enormous contributions based on seismic attributes for enhanced structural and stratigraphic interpretations within the Niger Delta basin to investigate the potentiality of hydrocarbon deposits (Ochoma, et al, 2023). Ochoma, et al, (2023) used the variance edge analysis to delineate the prominent and subtle faults in the area. The sweetness value ranges from 0 to 22,500. The high sweetness regions in the seismic data indicate high amplitude which indicates the presence of hydrocarbon-bearing sand units. The RMS amplitude values range from 0 to 13,000 in the reservoirs. The root mean square amplitude analysis also indicates the presence of hydrocarbon in

seismic data. The relative acoustic impedance analysis was used for delineating lithology variation in the seismic sections.

This study is taken from Fuba Field, Depobelt, Niger Delta, Nigeria. The ultimate deliverable of this study was seismic attributes analysis as a precursor for hydrocarbon indication of the area. The major components of this study are: (a) Well Correlation performed in order to determine the continuity of the reservoir sand across the field. (b) Seismic Interpretation which involves well-to-seismic tie, fault mapping, horizon mapping, time surface generation, depth conversion, generation of seismic attributes, seismic attributes analysis, prediction of reservoir properties from the seismic attributes and delineating hydrocarbon prospects using seismic attributes as direct hydrocarbon indicators (DHIs). This aids in giving more insight into seismic attributes analysis as a precursor for hydrocarbon indication.

2.0. Location and Geology of the Study Area

The proposed study area Fuba Field is located in the onshore Niger Delta region. Figure 1 shows the map of the Niger Delta oilfields showing the study area. The Niger Delta lies between latitudes 4° N and 6° N and longitudes 3° E and 9° E (Whiteman, 1982). The Delta ranks as one of the major oil and gas provinces globally, with an estimated ultimate recovery of 40 billion barrels of oil and 40 trillion cubic feet of gas (Adegoke et al., 2017). The coastal sedimentary basin of Nigeria has been the scene of three depositional cycles (Short and Stauble, 1967) [14].
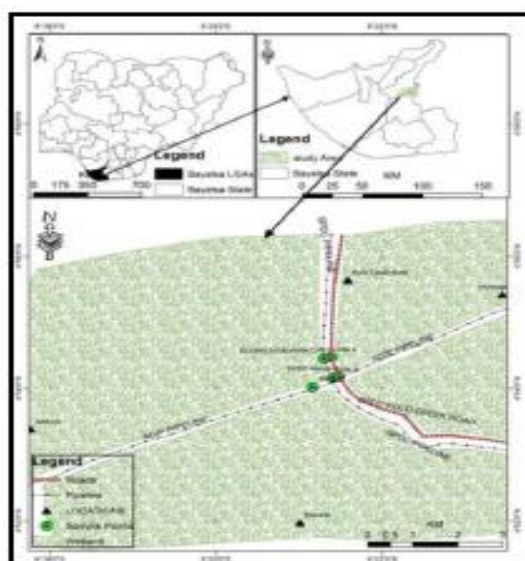

Figure 1. Map of Niger Delta Oilfields showing the location of Fuba Field

The first began with a marine incursion in the middle Cretaceous and was terminated by a mild folding phase in Santonian time. The second included the growth of a proto-Niger delta during the Late Cretaceous and ended in a major Paleocene marine transgression. The third cycle, from Eocene to Recent, marked the continuous growth of the main Niger delta. A new threefold lithostratigraphic subdivision is introduced for the Niger delta subsurface, comprising an upper sandy Benin Formation, an intervening unit of alternating sandstone and shale named the Agbada Formation, and a lower shaly Akata Formation. These three units extend across the whole delta and each ranges in age from early Tertiary to Recent. They are related to the present outcrops and environments of deposition. A separate member of the Benin Formation is recognized in the Port Harcourt area. It is Miocene-

Recent in age with a minimum thickness of more than 6,000ft (1829m) and made up of continental sands and sandstones (>90%) with few shale intercalations (Horsfall et al., 2017). Subsurface structures are described as resulting from movement under the influence of gravity and their distribution is related to growth stages of the delta (Ochoma et al., 2020). Rollover anticlines in front of growth faults form the main objectives of oil exploration, the hydrocarbons being found in sandstone reservoirs of the Agbada Formation. The oil in geological structures in the basin may be trapped in dip closures or against a synthetic or antithetic fault.

3.0. Methodology

3.1. Well-Log and Seismic Data Quality Control

Well correlation involves lithologic description, picking top and base of sand-bodies, fluid discrimination and then linking these properties from one well to another based on similarity in trends. Correlation of reservoir sands was achieved using the top and base of reservoir sands picked. The correlation process was possible based on similarity in the behaviour of the gamma ray log. In the Niger Delta, the predominant lithologies are sands and shales. In order to discriminate between these two lithologies in the subsurface, the gamma ray log is used. After defining the lithologies, the resistivity log was used for discriminating the type of fluid occurring within the pores in the rocks.

There are seven basic steps involved in seismic interpretation relevant to this study and they include well-to-seismic ties, fault Mapping, horizon mapping, time surface generation, velocity modeling, depth conversion and attributes generation. The sonic log, which is the reciprocal of velocity, was calibrated using the checkshot data. The calibration process is necessary in order to improve the quality of the sonic log because the sonic log is prone to washouts and other wellbore related issues. The results of calibrating the sonic log with the checkshot gives the calibrated sonic log.

The calibrated sonic log is used along with the density log to generate an acoustic impedance (AI) log. The acoustic impedance log is calculated for each layer of rock. The next step involves generating the reflectivity coefficient (RC) log. The RC is calculated and generated using the AI log. The RC log generated is then convolved with a wavelet to generate a synthetic seismogram which is comparable with the seismic data. The statistical wavelet utilized for convolution is extracted from the seismic data. The synthetic seismogram was generated. The mathematical expressions that govern the entire well-to-seismic tie workflow are presented below:

$$AI = \rho v \tag{1}$$

$$RC = \frac{\rho_2 v_2 - \rho_1 v_1}{\rho_2 v_2 + \rho_1 v_1} \tag{2}$$

$$\text{Synthetic Seismogram} = \frac{\rho_2 v_2 - \rho_1 v_1}{\rho_2 v_2 + \rho_1 v_1} * wavelet \tag{3}$$

where AI = acoustic impedance, RC = reflection coefficient, ρ = density; v = velocity.

Faults were identified as discontinuities or breaks in the seismic reflections. Faults were mapped on both inline and cross-line directions. Horizons are continuous lateral reflection events that are truncated by fault lines. The horizon interpretation process was conducted along both inline and crossline direction. At the end of the horizon mapping, a seed grid is generated which serves as an input for time surface generation. Time surfaces were generated using

the seed grids gotten from the horizon mapping process. The third order polynomial velocity model was generated and used to depth convert the time surfaces of the reservoirs of interest.

Petrel software platform 2017 was used for the 3D seismic interpretation, attribute visualization, and well logs data analysis. Among the seismic attributes that have been used in the visualization of the geology of the subsurface are variance, root mean square amplitude, maximum amplitude and relative acoustic impedance. The variance and relative acoustic impedance attributes analysis were applied to the seismic inline 8515 while root mean square amplitude and maximum amplitude were generated as surface attributes.

3.2. Determination of Root Mean Square (RMS) Amplitude

Root mean square (RMS) amplitude is used to obtain a scaled estimate of seismic trace envelope. It is obtained in the software by sliding a tapered window of N samples as the square root of the sum of all the trace value x squared. The RMS attribute computation in Petrel software makes use of the inbuilt formula:

$$X_{rms} = \sqrt{\frac{1}{N} \sum_{n=1}^{N} w_n x_n^2} \qquad (4)$$

where X_{rms} = root mean square amplitude, w_n = window values, N = number of samples in the window, x = trace value.

3.3 Variance (Edge Detection) Method

In the Petrel software, the variance attribute uses an algorithm that computes the local variance of the seismic data through a multi-trace window with user-defined size. The local variance is computed from horizontal sub-slices for each voxel. A vertical window was used for smoothing the computed variance and the observed amplitude normalized. The variance attribute measures the horizontal continuity of the amplitude that is the amplitude difference of the individual traces from their mean value within a gliding CMP window.

$$\sigma^2 = \frac{1}{n} \sum_{f_i=1}^{n} (x_i + x_m)^2 \qquad (5)$$

Where σ = standard deviation, σ^2 = variance, n = the number of observations, f_i = frequency, x_i = the variable, x_m = mean of x_i.

3.4. Determination of Relative Acoustic Impedance

The acoustic impedance inversion transforms the seismic data into an acoustic impedance model. The acoustic impedance of a media is given as equation (1). To measure acoustic impedance, it is necessary to use seismic inversion. It was assumed that the input seismic data has been processed to reduced noise and multiples, and also contains zero phase and large bandwidth. The seismic trace represents a band-limited reflective series;

$$f(t) = \frac{1}{2} \frac{\Delta \rho v}{\rho v} \qquad (6)$$

where $f(t)$ = seismic trace, $\Delta \rho v$ = the difference in the product of density and velocity. The integration of the seismic trace will provide a bandlimited estimate of the natural log of the acoustic impedance. Since the integration

of band-limited, the impedance will not have absolute magnitude values and consequently is only relative. Relative acoustic impedance is an estimated inversion computed by the integration of seismic trace accompany by a high cut Butterworth zero-phase filter. It is a simplified inversion and has been generated as an asynchronous attribute in the software. It enhances acoustic impedance contrast boundaries. The relative acoustic impedance (RAI) can be computed by integrating the real part of the seismic trace (Taner, 2001).

$$\ln(\rho v) = 2 \int_{t=0}^{t=1} f(T) dt \qquad (7)$$

Where $f(T)$ = real part of seismic trace. A Butterworth filter is then applied to remove long-wavelength trends that originated from the integration process (Schlumberger, 2007a).

$$BL(f) = \frac{1}{1 + (\frac{f}{f_H})^{2N}} \qquad (8)$$

where $BL(f)$ = band –limited signal in frequency; f_H = frequency cut-off value of 10 Hz, N = filter order of 3.

It is used for delineating sequence boundaries, unconformity surfaces, and discontinuities. The acoustic impedance may be related to the formation porosity and the presence of fluid in a hydrocarbon reservoir.

3.5. Determination of Maximum Amplitude

Amplitude is the deviation a wave from zero crossing. Maximum positive amplitude is referred to as peak value. The Maximum positive amplitude attribute computation in Petrel software makes use of the inbuilt formula:

$$y = A\sin(\omega t + \phi) = \qquad (9)$$

where A = Amplitude of the seismic wave, ϕ = Phase of the seismic wave, ω = Angular frequency of the seismic wave and t = time period.

4.0. Results and discussion

4.1. Reservoir Identification, Correlation and Well-To-Seismic Ties

The results for lithology and reservoir identification are presented in Figure 2. A total of fifteen sand bodies (A, B, C, D, E, F, G, H, I, J, K, L, M, N and O) were identified and correlated across all seven wells in the field. Three reservoir sands were selected for the purpose of this study (M, N and O). The resistivity logs which reveals the presence of hydrocarbons were used to identify the hydrocarbon bearing sands. On Figure 2, the sands are coloured yellow while shales are grey in colour. Figure 3 shows the quality of Well-1 checkshot utilized for well-to-seismic tie. The results for well-to-seismic tie conducted on Fuba field using density log, sonic log and checkshot of Well-1 is presented in Figure 4. An extended white 2 wavelet was used to give a near perfect match between the seismic and synthetic seismogram.

4.2. Fault and Horizon Interpretation

The results for the interpreted faults in Fuba field are presented in Figure 5 shows both synthetic and antithetic faults interpreted along seismic inlines. Faults are more visible along the inline direction because this direction

reveals the true dip position of geologic structures. The variance time slice was used to validate the interpreted faults as seen on Figure 6. All interpreted faults are normal synthetic and antithetic faults. A total of thirty-six faults were interpreted across the entire seismic data. Of the 36 interpreted faults, only F1 (synthetic fault) and F16 (antithetic fault) faults are regional, running from the top to bottom across the field. Hence, these faults play significant roles in trap formation at the upper, middle and lower sections of the field.

The results for the interpreted seismic horizons (Horizon M, Horizon N and Horizon O) are also presented in Figure 6. On these horizons, the fault polygons were generated and eliminated. The horizons were used as inputs for the generation of reservoir time surfaces. The reservoir time surfaces (M, N and O reservoirs) reveal that the reservoir structure is a collapsed crest, bounded by two regional faults (F1 and F16). Reservoir M, N and O time surfaces are truncated by two bounding faults and three minor inter-reservoir faults. The fault supported collapsed crestal structures are the closures identified on reservoir M, N and O reservoir surfaces respectively. The similarity in structure on reservoir M, N and O reveals that the field is structurally controlled by faults. The third order polynomial velocity function used for depth converting the studied surfaces is presented in Figure 7. The depth converted reservoir M, N and O surfaces are presented in Figures 8, 9 and 10 for the third order polynomial velocity function. The depth structure maps reveal that the reservoirs are anticlinal and fault supported. Reservoir M is found at a shallower depth from 10937 to 10997 ft, reservoir N is found at a depth ranging from 11213 to 11241 ft while reservoir O is found at a deeper depth ranging from 11681 to 11871 ft respectively.
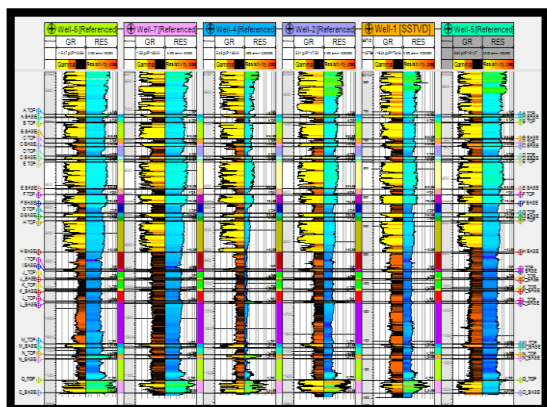

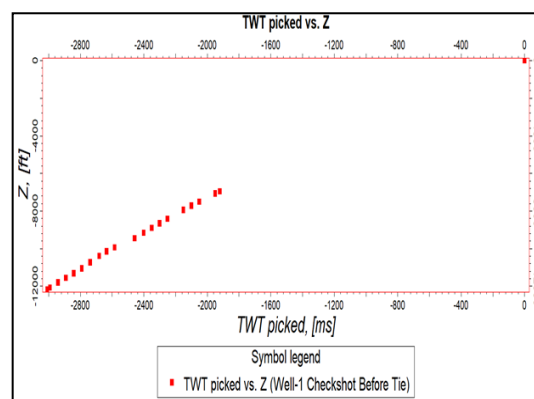**Figure 2.** Well Section Showing Reservoir Identified and Correlated Across Fuba Field

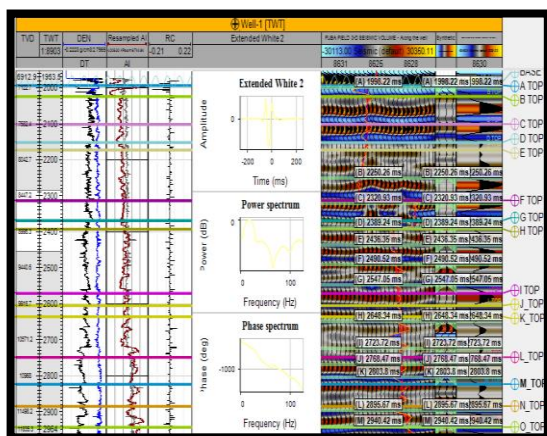**Figure 3.** Quality of Well-1 Checkshot Utilized for Well-to-seismic Tie

Figure 4. Synthetic Seismogram Generation and Well-to-seismic Tie Conducted for Fuba Field using Well-1 Checkshot
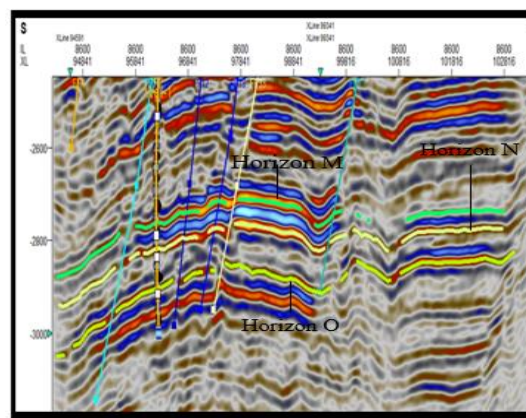

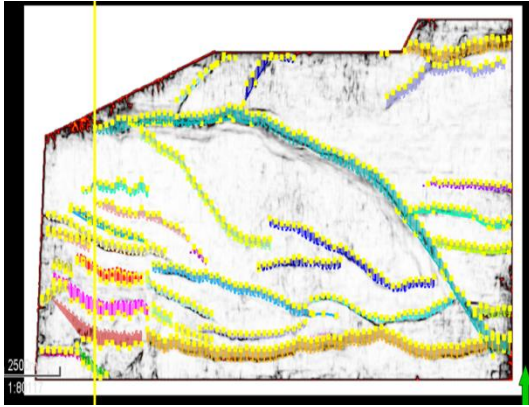**Figure 5.** Faults and Horizons Interpreted Along Seismic Inline section

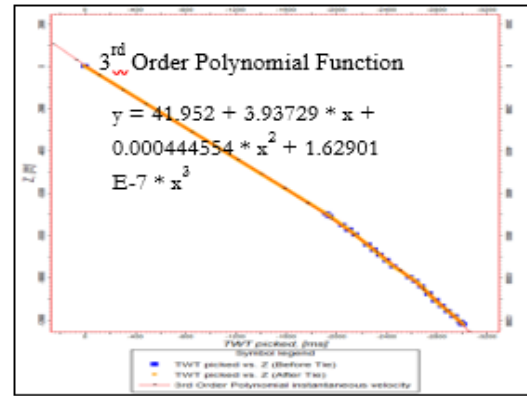**Figure 6.** Interpreted Faults Displayed on the Variance Time Slice

Figure 7. Third Order Polynomial Velocity Model Utilized for Converting Reservoir Surfaces from Time to Depth
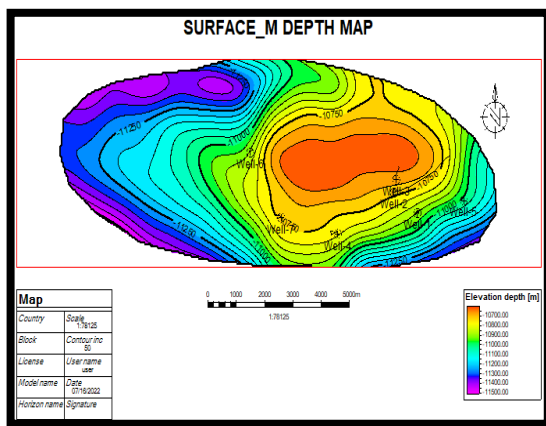

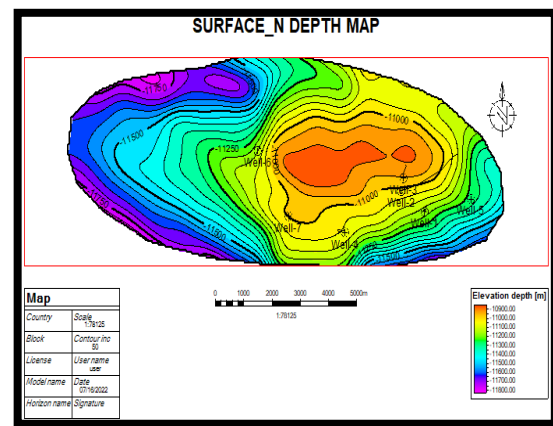**Figure 8.** Reservoir Surface for Depth Surface M
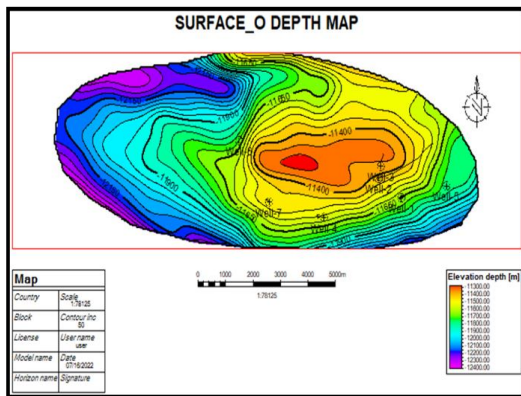

Figure 9. Reservoir Surface for Depth Surface N

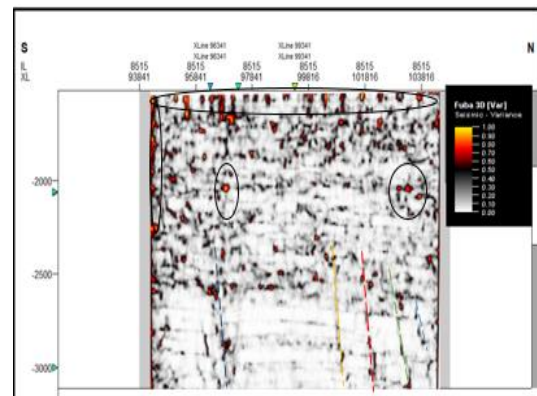**Figure 10.** Reservoir Surface for Depth Surface O

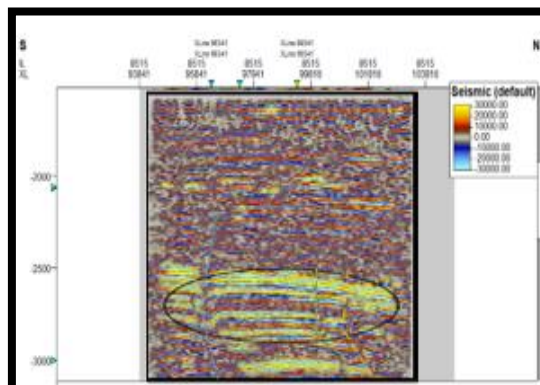**Figure 11.** Variance Edge inline 8515

Figure 12. Relative acoustic impedance Inline 8515

Figure 13. Generated Amplitude Maps for Reservoir Surface M (a) Maximum Amplitude Map, (b) RMS Amplitude Map Showing Identified Hydrocarbon Leads (A, B, C, D and E) away from the Producing Zone "X"

Figure 14. Generated Amplitude Maps for Reservoir Surface N (a) Maximum Amplitude Map, (b) RMS Amplitude Map Showing Identified Hydrocarbon Leads (A, B, C and D) away from the Producing Zone "X"
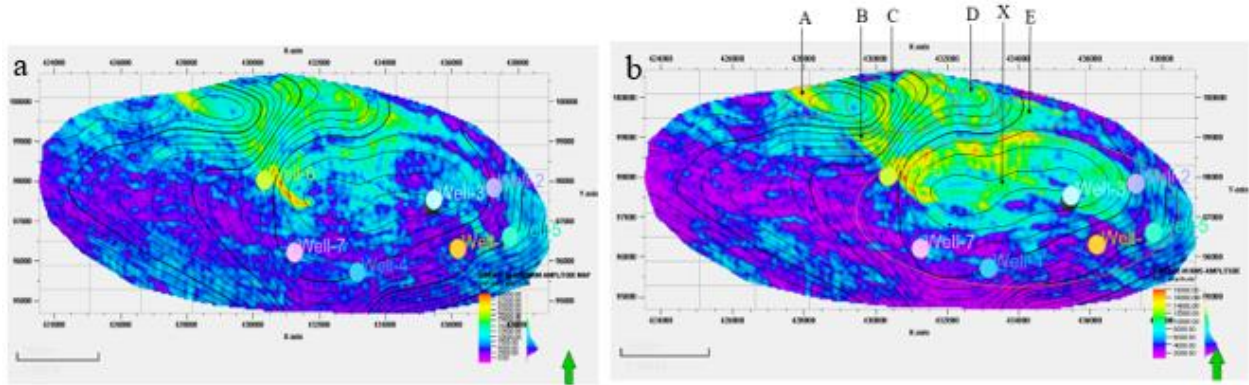

Figure 15. Generated Amplitude Maps for Reservoir Surface O (a) Maximum Amplitude Map, (b) RMS Amplitude Map Showing Identified Hydrocarbon Leads (A, B, C, D and E) away from the Producing Zone "X"
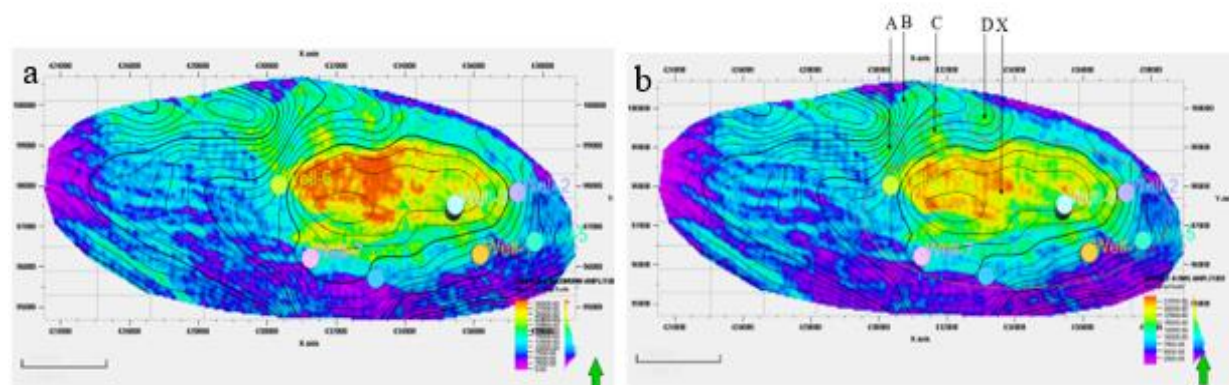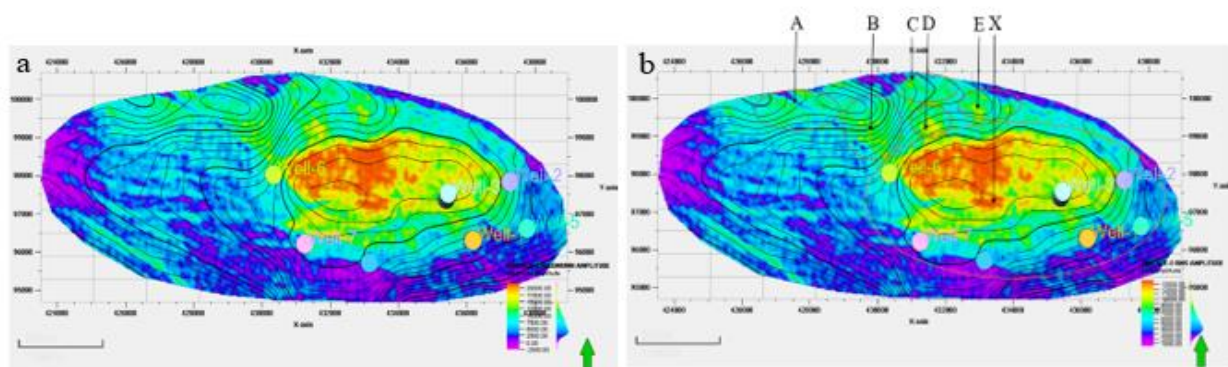
4.3. Seismic Attributes

A series of seismic attributes such as variance edge, maximum amplitude, relative acoustic impedance and RMS amplitude were generated in Schlumberger's Petrel® software interface to investigate potential structural and stratigraphic controls and also delineate hydrocarbon prospects within the study area. Figure 11 shows the computed variance attributes of the seismic section. The variance values range from 0.0 to 1.0. Values of variance equal to 1 represent discontinuities while a continuous seismic event is represented by the value of 0. The high values are denoted with red to yellow colorations. On the variance map, the areas dotted with blue, green, orange and pink colored lines signify values that correspond to the location of the discontinuity. The discontinuities may be

interpreted as faults and boundaries as shown by the lines drawn on the variance attribute map (Law, and Chung, 2006).The variance edge enhanced the faults or sedimentological bodies within the seismic data volume. Furthermore, several bright spots are also delineated (in black circles and black ovals) which indicate high reflectivity sediments compared to their surroundings. These bright spots are an indication that a potential hydrocarbon trap might exist in the area. The darkest regions in the seismic section, which make vertical stripes, may be interpreted as faults or fractures. The zones with low variance values are due to similar seismic traces. Areas with red patches represent lineaments/discontinuities while grey areas represent the structural framework of the field.

The variance attribute is edge imaging and detection techniques. It is used for imaging discontinuity related to faulting or stratigraphy in seismic data. Variance attribute is proven to help in imaging of channels, fault zones, fractures, unconformities and the major sequence boundaries (Pigott, 2013).

The relative acoustic impedance generated in the study area is shown in Figure 12. Based on the map, the yellow and red colours represent the highest relative impedance (in black circles) while the lowest relative impedance is represented by the blue colour. The relative acoustic impedance attribute represents apparent acoustic impedance or physical property contrasts. It is commonly used for lithology discrimination, thickness variation and sequences boundaries indicators associated with high contrasts in acoustic impedance values. It may also indicate unconformity surfaces, discontinuities, porosity and the presence of hydrocarbon in a reservoir (Oyeyemi and Aizebeokhai 2015). The high relative acoustic impedance values are associated with shalier facies while lower values correspond to sand intervals (Alabi, and Enikanselu, 2019; Suarez, et al, 2008). The high relative acoustic impedance may also be interpreted as sequences boundaries.

The maximum amplitude map generated for all the studied surfaces (surface M, N and O) showed that strong amplitude anomalies exist at the central part of the field and parts of northeast, northwest, southwest and southeast sections (Figures 13(a), 14(a) and 15(a). The parts of the field where these strong amplitude anomalies were observed corresponds to the observed anticlinal structure in the field. Other parts of the field where the amplitude anomalies were observed also correspond to the identified structural closures found in the field. Results indicate that strong amplitude anomalies are structurally controlled as they are seen occurring near faults on structural maps. The maximum amplitude and RMS attributes maps generated for reservoirs of interest presented in Figures 13, 14 and 15 were seen to have similar patterns of bright spot anomaly, which are likely associated with of facies and/or fluid content (Raef, et al, 2016). In addition, these anomalies are seen on structural high, which suggested prospect conformity with regional structural high.

The results of the analysis of the RMS amplitude maps is presented in table 1. The RMS amplitude values range from 0 (purple) to 13,000 (red) in reservoir M, from 0 (purple) to 12,000 (red) in reservoir N and 0 (purple) to 9,000 (red) in horizon O. The red-yellowish colour represents hydrocarbon sands. Some of these hydrocarbon sands were not detected in the original seismic section. The observed changes may be due to changes in lithology or fluid content.

The RMS attribute is related to the variations in acoustic impedance. The higher the acoustic impedance values, the higher the RMS amplitude. The high values of RMS amplitudes may also be related to high porous sands, which are

potential hydrocarbon reservoirs. RMS amplitude is similar to reflection strength and it is used in seismic exploration for delineating bright spots and amplitude anomalies (Fozoa et al, 2018; Opara, and Osaki, 2018). The RMS amplitude is used for identifying coarser-grained facies, compaction related effects, and unconformities. The high values of RMS amplitudes circled (in orange circles) in the maps are interpreted as high porosity lithologies, such as porous sands. These high RMS amplitude segments are potential high quality hydrocarbon reservoirs. The high amplitude (in orange circles) in the seismic data conforms to the structures and confirms the presence of hydrocarbon (Ajisafe, and Ako, 2013). The high amplitude ranges from light blue to yellow and red coloration. Root mean square amplitude is used as a good indicator of the presence of hydrocarbon in seismic data.

Table 1. RMS Amplitude Values for the Reservoir Surfaces

Reservoir	Range of RMS Amplitude Values
Reservoir-M	0 – 13,000
Reservoir _N	0 – 12,000
Reservoir _O	0 – 9,000

4.4. Hydrocarbon Prospect Identification

Evaluation of hydrocarbon prospectivity reveals that the study area has high fault density, which makes trapping structures available for hydrocarbon accumulation, thus providing possible hydrocarbon leads. Within the three reservoir intervals, the central part, northeast and southeast in an orange oval denoted with "X" has been previously evaluated and seen to have potential trap that turned into an oil/gas field when drilled, hence a good hydrocarbon prospect. This prospect is quite evidenced from the depth maps and several amplitude maps that were generated. Prospect "X" shows booming amplitude that is structurally controlled, which has given rise to several drilling campaigns within the zone (Figures 13, 14 and 15). However, away from the "X" prospect this study has been able to identify other prospective zone characterized by good amplitude response and trapping structures. The root-mean-square amplitude attribute was used for the identification of prospective zones because it is more sensitive to direct hydrocarbon indicators (DHIs) than others and its pattern of bright spot anomaly superposition on the structural closures are discrete. Five hydrocarbon prospective zones each were identified for reservoirs M and O while four hydrocarbon prospective zones were identified for reservoir N (Figures 13(b), 14(b) and 15(b)). All the identified prospective zones in orange circles (A, B, C, D and E) in the reservoirs tops show two-way fault dependent closures. These been classified a hydrocarbon leads, since there are good trapping structures and hydrocarbon presence. Within reservoir M, zones A, B and C rank the best hydrocarbon lead considering the well-developed entrapment mechanisms for hydrocarbon accumulation and moderate to high amplitude response. Within reservoir N, zone C ranks the best hydrocarbon lead considering the well-developed entrapment mechanisms for hydrocarbon accumulation and moderate to high amplitude response. For reservoir O, zones B, D and E rank the best hydrocarbon lead considering the well-developed entrapment mechanisms with moderate to high amplitude response. This study has shown that, away from the producing zone (prospect "X," which is

common to all the three reservoir tops and characterized by anticlinal structure at the central part of the field), the application of seismic attribute analysis has unraveled several hydrocarbon prospective zones that could be further revalidated and evaluated to hydrocarbon prospects.

5.0. Conclusion

A total of fifteen sand bodies (A, B, C, D, E, F, G, H, I, J, K, L, M N and O) were identified and correlated across all seven wells in the field. All interpreted faults are normal synthetic and antithetic faults. A total of thirty-six faults were interpreted across the entire seismic data. Of the thirty-six interpreted faults, only F1 (synthetic fault) and F4 (antithetic fault) faults are regional, running from the top to bottom across the field. Hence, these faults play significant roles in trap formation at the upper, middle and lower sections of the field. Three horizons (M, N and O) were selected for the study.

The seismic attributes interpreted include variance, relative acoustic impedance, maximum amplitude and root mean square amplitude. The variance values ranges from 0.0 to 1.0. The variance edge revealed the subtle structures and faults in the seismic section. The relative acoustic impedance analysis was used for delineating lithology variation in the seismic sections. The RMS amplitude values range from 9,000 to 13,000 in the reservoirs. The RMS amplitude, maximum amplitude and relative acoustic impedance results highlighted the hydrocarbon zones. The maximum amplitude and RMS attributes maps generated for reservoir tops of interest were seen to have similar pattern of bright spot anomaly. These amplitude anomalies served as direct hydrocarbon indicators (DHIs), unravelling the presence and possible hydrocarbon prospective zones. Also, it indicates that away from the producing zone that there exist other hydrocarbon prospective zones. Several prospective hydrocarbon leads identified within three studied reservoirs (M, N, and O) intervals show good trapping structures such as anticlines which support hydrocarbon accumulation. Fault and horizon interpretation revealed that closures found on M, N and O reservoirs are collapsed crestal structures bounded by the two major faults. The depth structure maps reveal that the reservoirs are anticlinal and fault supported. Reservoir M is found at a shallower depth from 10937 to 10997 ft, reservoir N is found at a depth ranging from 11213 to 11241 ft while reservoir O is found at a deeper depth ranging from 11681 to 11871 ft respectively. Extracted amplitude maps revealed that zones with good amplitude response, which indicates the presence hydrocarbon bearing reservoir section, are structurally controlled. The study has demonstrated that the application of seismic amplitude attribute, which offers insight on hydrocarbon presence and distribution of reservoir sand, could help unravel prospective intervals where there are no well controls. Hydrocarbon exploration and development risks can be reduced greatly with the outcome of seismic attributes extraction and analysis. It is recommended that careful quality control of the updated velocities using existing horizons should be performed so that the resulting velocity maps can be used for accurate depth conversion. Finally, fault seal analysis should be carried out to confirm that the suspected trapping faults are not leaking in which case they serve as conduits for hydrocarbon migrations rather than lateral barriers to hydrocarbon escape.

References

[1] Liner, C.L. (2004). Elements of 3D Seismology, 2nd Edition. Penn Well Books, Tulsa, OK.

[2] Oyeyemi, K.D. & Aizebeokhai, A.P. (2015). Seismic Attributes Analysis for Reservoir Characterization; Offshore Niger Delta. Petroleum and Coal, 57(6): 619–628

[3] Adewoye, O., Amigun, J.O. & Afuwai, C.G. (2015). Lithostratigraphic Interpretation and Seismic Attributes Analysis for Reservoir Characterization in Some Parts of Niger Delta. Petroleum and Coal, 57(1): 76–84.

[4] Steiner, W. & Lockhart, J., (1988). Seismic Classification and Reservoir Volume Analysis of the Upper Wahoo Oil Field, www.petrobjects.com/papers.

[5] Allstair, R.B. (2011). Interpretation of 3D seismic data, 7th edn. The American Association of Petroleum Geologists and Society of Exploration Geophysics, Tusla.

[6] Avseth, P., Mukerji, T. & Mavko, G. (2005). Quantitative Seismic Interpretation. Cambridge University Press, Cambridge, Pages 168–170.

[7] Omoja U.C. & Obiekezie T.N. (2019). Application of 3D Seismic Attribute Analyses for Hydrocarbon Prospectivity in Uzot-Field, Onshore Niger Delta Basin, Nigeria. International Journal of Geophysics, Pages 1–11.

[8] Pramanik, A.G., Singh, V., Srivastava, A.K. & Rakesh, Katiyar (2002). Stratigraphic Inversion for Enhancing Vertical Resolution. Geohorizons, 7(2): 8–18

[9] Van, R.P. (2000). The Past, Present, and Future of Quantitative Reservoir Characterization. Leading Edge, 19(8): 878–881.

[10] Vig, R., Singh, V., Kharoo, H.L., Tiwari, D.N., Verma, R.P. Chandra, M. & Sen, G. (2002). Post Stack Seismic Inversion for Delineating Thin Reservoirs: A Case Study. In: Proceedings of 4th conference and Exposition in Petroleum Geophysics (Mumbai-2002) held during January 7–9, Pages 287–291.

[11] Chopra, S. & Marfurt, K.J. (2005). Seismic Attributes—a Historical Perspective. Geophysics, 70(5): 3–28.

[12] Ochoma, U, Tamunobereton-ari I., Amakiri, A.R.C. Sigalo, F.B. & Horsfall O.I. (2023). 3-D Seismic Attributes Analysis for Enhanced Hydrocarbon Prospect Definition of Onshore Fuba Field Niger-Delta, Nigeria. IOSR Journal of Applied Geology and Geophysics, 11(2): 63–70.

[13] Whiteman, A. (1982). Nigeria: Its Petroleum Ecology Resources and Potential. London, Graham and Trotman.

[14] Adegoke, O.S., Oyebamiji, A.S., Edet, J.J, Osterloff, P.L. & Ulu, O.K (2017). Cenozoic Foraminifera and Calcareous Nannofossil Biostratigraphy of the Niger Delta, Elsevier, Cathleen Sether, United States.

[15] Short, K.C. & Stable A.J. (1967). Outline of Geology of Niger Delta. Bulletin of America Association of Petroleum Geologists, 51(5): 761–779.

[16] Horsfall, O.I., Uko, E.D., Tamunoberetonari I. & Omubo-Pepple, V.B. (2017). Rock-Physics and Seismic-Inversion Based Reservoir Characterization of AKOS FIELD, Coastal Swamp Depobelt, Niger Delta, Nigeria. IOSR Journal of Applied Geology and Geophysics, 5(4): 59–67.

[17] Ochoma, U., Uko E.D. & Horsfall, O.I. (2020). Deterministic Hydrocarbon Volume Estimation of the Onshore Fuba Field, Niger Delta, Nigeria. IOSR Journal of Applied Geology and Geophysics, 8(1): 34–40.

[18] Taner (2001). Seismic Attributes: Canadian Society of Exploration Geophysicists Recorder, 26(9): 48–56.

[19] Law W.K. & Chung A.S.C. (2006). Minimal Weighted Local Variance as Edge Detector for Active Contour Models. In: Narayanan et al. PJ (Eds), Accv 2006, LNCS 3851, Pages 622–632.

[20] Pigott. J.D., Kang, M.I.H. and Han, H.C. (2013). First Order Seismic Attributes for Clastic Seismic Facies Interpretation: Examples from the East China Sea. Journal of Asian Earth Science, 66: 34–54.

[21] Oyeyemi K.D. & Aizebeokhai A.P. (2015). Seismic Attributes Analysis for Reservoir Characterization; Offshore Niger Delta. Petroleum Coal, 57(6): 619–628.

[22] Alabi, A.A. & Enikanselu, P.A. (2019). Integrating Seismic Acoustic Impedance Inversion and Attributes for Reservoir Analysis Over 'DJ' Field, Niger Delta. Jour of Petroleum Exploration Production Tech., 9: 2487–2496.

[23] Suarez Y., Marfurt K.J. & Falk M. (2008). Seismic Attribute-Assisted Interpretation of Channel Geometries and Infill Lithology: A Case Study of Anadarko Basin Red Fork channels. In 78th Annual International Meeting, SEG, Pages 963–996.

[24] Raef, A.E., Meek, T.N. & Totten, M.W. (2016). Applications of 3d Seismic Attribute Analysis in Hydrocarbon Prospect Identification and Evaluation: Verification and Validation Based on Fluvial Palaeochannel Cross-Sectional Geometry and Sinuosity, Nesscounty, Kansas, USA, Marine and petroleum geology, 73: 21–35.

[25] Fozao, K.F., Fotso, L., Djieto-Lordon, A. & Mbeleg, M. (2018). Hydrocarbon Inventory of the Eastern Part of the Rio Del Rey Basin Using Seismic Attributes. Journal of Petroleum Exploration and Production Technology, 8: 655–665.

[26] Opara, A.I. & Osaki, L.J. (2018). 3-D Seismic Attribute Analysis for Enhanced Prospect Definition of "Opu Field", Coastal Swamp Depo Belt Niger Delta, Nigeria. Journal of Applied Science, 18: 86–102.

[27] Ajisafe, YC & Ako, BD (2013). 3-D Seismic Attributes for Reservoir Characterization of 'Y' field, Niger Delta, Nigeria. IOSR Journal of Applied Geology and Geophysics, 1: 23–31.